Selfconsistent RF Driven and Bootstrap Currents

Y. Peysson 1), J. Decker 2), A. Bers 2), A. K. Ram 2)

1) Association Euratom – CEA, CEA/DSM/DRFC
CEA-Cadarache, 13108 S^{t} Paul-lez-Durance (France)

2) Plasma Science and Fusion Center
Massachusetts Institute of Technology, Cambridge, MA 02139 U.S.A.

E-mail contact of main author: yves.peysson@cea.fr

Abstract: In order to achieve steady-state high performance regimes in tokamaks, it is important to sustain and control the pressure and magnetic shear profiles in high bootstrap current plasmas. RF waves can be used to achieve such a goal. Then the bootstrap current fraction must be calculated selfconsistently with RF induced currents, taking into account possible synergistic effects resulting from the distortion of the electron velocity-space distribution. Results obtained with a new 3-D code that solves the electron drift kinetic equation to study the synergistic effects are presented. While synergism between bootstrap and LH-driven currents remains modest, it may reach up to 30-40% for the case of EC current drive provided the plasma parameters are properly chosen.

1. Introduction

In advanced scenarios, radio frequency (RF) induced currents have to be calculated self-consistently with the bootstrap current, thus taking into account possible synergistic effects resulting from the momentum space distortion of the electron distribution function f_e. Since RF waves can cause the distribution of electrons to become non-Maxwellian, the associated changes in parallel diffusion of momentum between trapped and passing particles can be expected to modify the bootstrap current fraction; conversely, the bootstrap current distribution function can enhance the current driven by RF waves.

2. Drift kinetic formulation

We follow the development in [1] for finding the electron momentum distribution function in the selfconsistent interaction of RF current drive and bootstrap current. This approach solves the electron drift kinetic equation

$$\frac{v_\theta}{r}\frac{\partial f}{\partial \theta} + v_{Dr}\frac{\partial f}{\partial r} = C(f) + Q(f)$$

where $C(f)$ is the relativistic Fokker-Planck collision and $Q(f)$ is the quasilinear RF diffusion operator. Here, (r,θ) are the radial and poloidal positions, v_θ is the velocity along the poloidal field lines and v_{Dr} is the drift velocity across the field lines. An approximate formulation, based on an expansion in the small parameter $\delta = \tau_{t,b}/\tau_{Dr}$, where $\tau_{t,b}$ is the electron's transit or bounce time, and τ_{dr} is a typical time for the electron radial drift due to magnetic field gradient and curvature, is used to determine the electron distribution function in the low collisionality regime. In the limit $\delta << 1$, it can be shown that f may be expressed as $f \approx f_0 + \delta f_1 = f_0 + \tilde{f} + g$, where $\tilde{f}$ is the perturbation due to radial drift and gradients, and g is the response of the plasma due to collisions and RF fields. The first order term f_0 is determined by solving the steady-state 3-D relativistic bounce-averaged Fokker-Planck equation

$$\{C(f_0)\}+\{Q(f_0)\}=0$$

$\tilde{f}$ is given by $\tilde{f}=-\frac{v_{//}}{\Omega_\theta}\frac{\partial f_0}{\partial r}$ where Ω_θ is the poloidal gyrofrequency and $v_{//}$ the particle velocity along the magnetic field line, and *g* is determined from

$$\{C(g)\}+\{Q(g)\}=-\{C(\tilde{f})\}-\{Q(\tilde{f})\}$$

where *{ }* denotes the bounce-averaging operation.

3. Numerical implementation

The numerical solution of the set of equations has been carried out in the small inverse aspect ratio limit $\varepsilon = r/R_0 << 1$ for circular cross-section plasmas, using the 3-D Fokker-Planck solver DKE [2,3]. This fully implicit code, written in MatLab® matrix language, is used to study the interaction between the bootstrap current (BC) and the lower hybrid driven current (LHCD), the BC and the electron cyclotron driven current (ECCD), and the the BC and the Ohkawa driven current (OKCD) [4].

This code has been benchmarked against neoclassical resistivity calculations [5] and bootstrap current calculations [6,7,8] (Fig. 1). A departure from the calculations of Ref. [8] arises at large *r/a* because the condition $\varepsilon << 1$ is not well satisfied. The results of the code have also been compared with previous simulations applying to the case of a runaway discharge. It has been shown that the presence of a tail of fast electrons accelerated by the Ohmic electric field could significantly improve the bootstrap current [9]. As shown in the Fig. 2, similar results are obtained with our code. The slight difference may results from the fact that the dynamics of the electrons is described in the whole momentum space, rather at the trapped/passing boundary only, as done in [9].

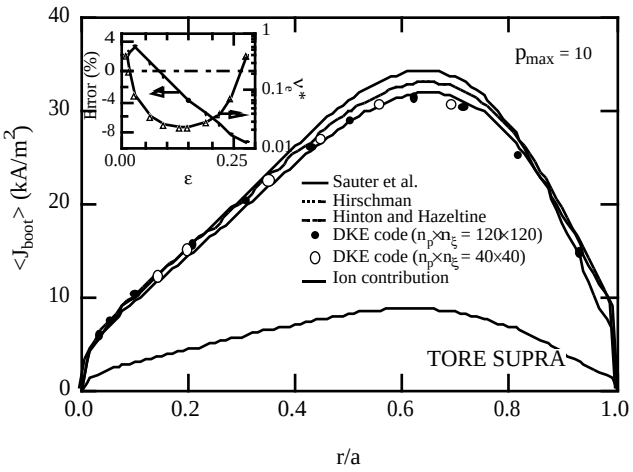

Fig. 1. Bootstrap current comparison between the code and theoretical predictions. The relative error for the electron component with the law given by Ref. [8] is presented in the insert, as well as the plasma collisionnality [8]. Simulations are done for a typical TORE SUPRA tokamak discharge

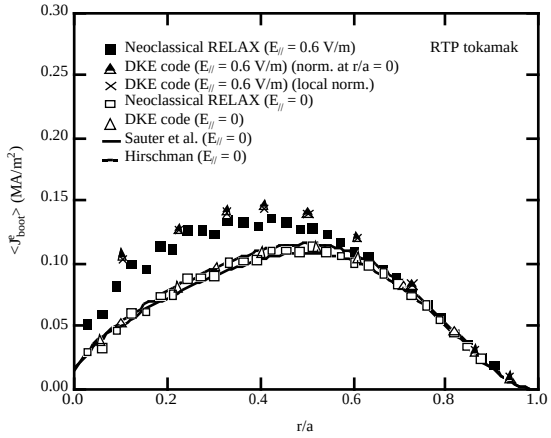

Fig. 2. Simulation of a run-away discharge on the RTP tokamak [9]. The bootstrap current is increased by 40% at r/a = 0.3. The method used with RELAX code [9] that singles out the term contributing to the boostrap current at the trapped/passing boundary gives similar results to the new approach [4]

The code has also been successfully benchmarked against other codes for LHCD and ECCD calculations, not including the interaction with the bootstrap current. The radial transport of the fast electrons and the role of the toroidal magnetic ripple in fast electron losses can also be investigated [10].

4. Self-consistent current calculations

The code DKE is used to compute the following flux surface averaged quantities: the RF current density $\langle J_{RF} \rangle$ and the density of power absorbed $\langle P_{RF} \rangle$ in the absence of bootstrap current; the bootstrap current density $\langle J_B \rangle$ in the absence of RF; the self-consistent (RF and Bootstrap) total current density $\langle J \rangle$ and total density of power absorbed $\langle P \rangle$. The synergistic current density is given by $\langle J_S \rangle = \langle J \rangle - (\langle J_{RF} \rangle + \langle J_B \rangle)$, and the figure of merit for the current drive is taken as $\eta = [(\langle J \rangle - \langle J_B \rangle)/\langle P \rangle]$. This is compared with $\eta_{RF} = \langle J_{RF} \rangle / \langle P_{RF} \rangle$. The results are illustrated for high performance scenarios in Alcator C-MOD [11]. In our studies the radial position is chosen to be $r/a=0.7$ where the peak RF current drive is expected. At this location, density and temperature are $1.8\times10^{+20}\ m^{-3}$ and $2.1\ keV$, respectively. We then find that $J_B=3.57\ MA.m^{-2}$.

4.1 Lower Hybrid current drive (LHCD)

The LH power spectrum is assumed to be constant in $k_{//}$ between two limits fixed by accessibility and by linear Landau damping (typically $\frac{p_{//\min}}{p_{Te}} \approx 3.5$). The normalized LH quasilinear diffusion coefficient is chosen to be $D_0^{LH} = 1.0 \nu_e p_{Te}^2$ which corresponds to an incoming LH power P_{LH} of 2 MW. A parametric study of the synergism shows that the synergistic current increases linearly with the temperature gradients but is independent of density gradients. This confirms the analytical results obtained in the Lorentz limit $Z_i >> 1$ [1] :

$$\frac{\langle J_S \rangle}{\langle J_{LH} \rangle} \approx \frac{1}{2} \sqrt{\varepsilon} \rho_\theta \frac{d \ln T_e}{dr} \left(\frac{p_{//\min}}{P_{Te}} \right)^3$$

In Fig. 3 we plot contours of the synergistic fraction of the current $\langle J_S \rangle / \langle J_{LH} \rangle$, and of the figure of merit η, for various temperature and density gradients ($T_e \propto \left(1-(r/a)^2\right)^{\alpha_T}$, $n_e \propto \left(1-(r/a)^2\right)^{\alpha_n}$). If the temperature gradient were made twice as steep, the bootstrap current would increase by 80% and the synergistic fraction would rise accordingly from 5% to 12% of the LH driven current.

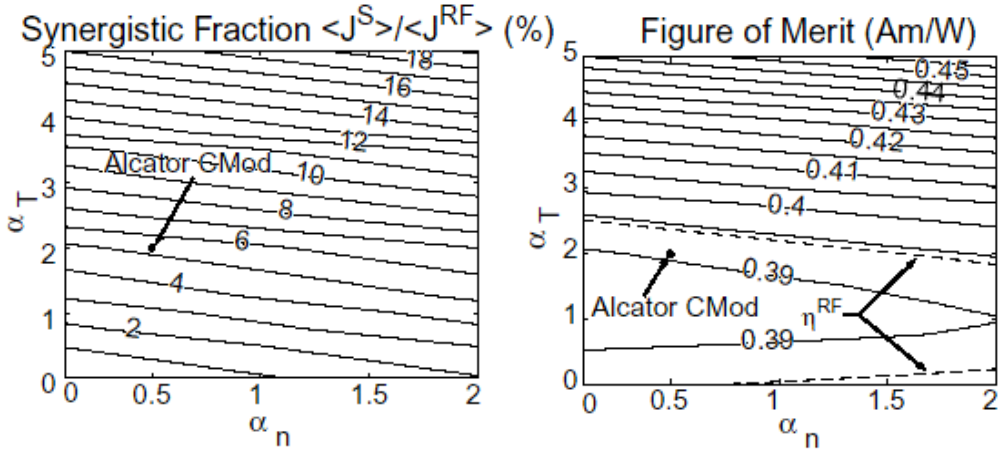

Fig.3. Synergistic fraction and figure of merit for the LH current drive problem at r/a = 0.7 (C-MOD)

Correspondingly, there is an 8% increase in the figure of merit.

4.2 Electron Cyclotron current drive (ECCD, OKCD)

ECCD at second harmonic with X-Mode excitation is considered, assuming a Gaussian power spectrum centered around $N_{//0}$ with a width $\Delta N_{//} = 0.02$. The maximum value of the EC diffusion coefficient for an incoming power P_{EC} of 10 MW is $D_0^{EC} = 0.14\nu_e p_{Te}^2$. The study is restricted to absorption on the low-field side (LFS) only. ECCD far off axis *(r/a = 0.7)* on the LFS is known to lead to poor CD efficiency due to the Ohkawa effect generated by a large number of trapped electrons. However, it is possible to use the Ohkawa current in a positive way, by launching waves with $N_{//0} < 0$, and adjusting the wave parameters so that the EC diffusion region in velocity space is located just below the trapped-passing boundary. Electrons are then mostly diffused into the trapped region and the Ohkawa effect becomes dominant. This is referred as the Ohkawa method for ECCD, and here noted as OKCD. The wave parameters $N_{//}$ and $2\omega_{ce}/\omega$ determine the location of the EC diffusion region in momentum space, and can be varied so as to optimize the current driven by either ECCD ($N_{//0} = 0.28$, $2\omega_{ce}/\omega = 0.97$) or OKCD ($N_{//0} = -0.30$, $2\omega_{ce}/\omega = 0.98$). The self-consistent calculation of ECCD with BC is performed using these optimized parameters and the results are presented in Table 1. A much larger current density is obtained for OKCD than for ECCD. In addition, the figure of merit is better, thus making OKCD more attractive than ECCD for off-axis CD on the LFS. A synergism is found both for ECCD and for OKCD, but the synergistic fraction of the current is much larger for ECCD (28%) than for OKCD (5%). In contrast to LHCD, synergism is also obtained in the figure of merit (25% increase in η for ECCD, and 5% in OKCD). The physical mechanism of the synergism between ECCD or OKCD and the bootstrap current can be visualized in a 2-D contour plot of the perturbed distribution $\delta f_1 = \tilde{f} + g$, generated by the radial drifts, as displayed in Fig. 4. In the case of ECCD, the synergism can be simply interpreted as the Fisch-Boozer effect on the « bootstrap » distribution. The Ohkawa effect on δf_1 is however different from f_0 because δf_1 is mostly negative for $p_{//} < 0$. Indeed, the synergism between OKCD and bootstrap current is a competition between a negative effect of EC induced electron trapping where $\delta f_1 < 0$ and $p_{//} < 0$, and a positive effect due the asymmetry in δf_1 , which leads to an increase in δf_1 where $p_{//} > 0$.

ECCD	EC	EC + Syn.
$\langle J \rangle$ $(MA.m^{-2})$	0.49	0.62
$\langle P \rangle$ $(MW.m^{-3})$	22.1	22.6
η *(Am/W)*	0.022	0.028

OKCD	OK	OK + Syn.
$\langle J \rangle$ $(MA.m^{-2})$	12.37	12.96
$\langle P \rangle$ $(MW.m^{-3})$	278.8	276.3
η *(Am/W)*	0.044	0.047

Table 1: ECCD and OKCD results at r/a = 0.7 (C-MOD)

5. Conclusion and prospects

A new two-dimensional code that allows fast selfconsistent calculations of the bootstrap current in the presence of RF waves has been written. It has been shown that the synergism between bootstrap and LH or EC driven currents could be a large fraction of the RF driven component, under the condition of the bootstrap current level is high. For LHCD, the synergism concerns the driven current but not the CD efficiency. Improvement is well understood by a simple analytical model. Conversely, the ECCD efficiency is higher when bootstrap current is accounted in the calculations. Further work remains to be done for an arbitrary plasma equilibrium, and high inverse aspect ratio.

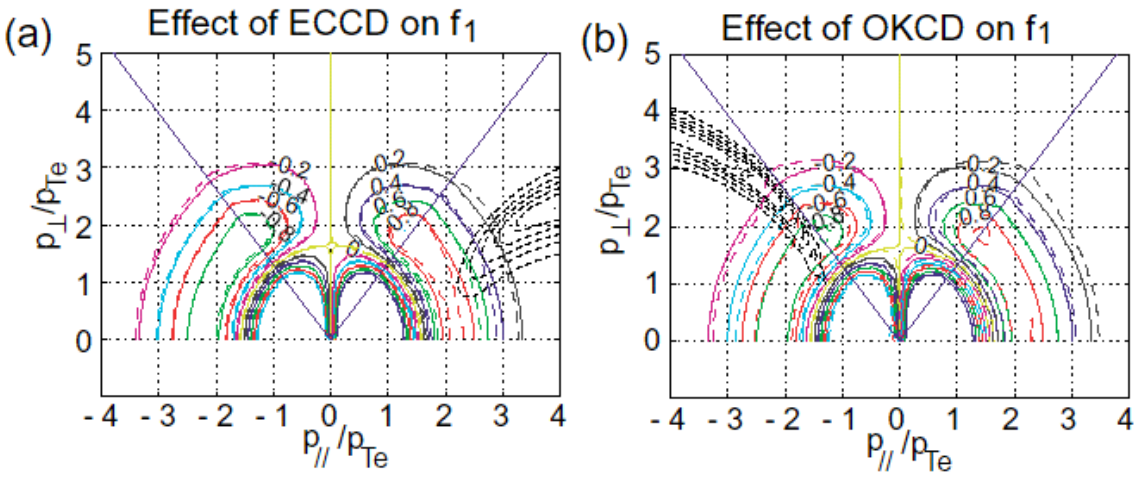

Fig. 4. 2-D contour plots of the perturbed distribution δf_1 generated by radial drifts with (dashed lines) and without (solid lines) for ECCD (a) or OKCD (b). Thin dashed contours correspond to EC quasilinear domains.

*Work supported in part by U.S. DoE Grant DE-FG02-91ER-54109 and U.S. DoE Cooperative Grant DE-FC02-99ER-54512.

[1] SCHULTZ S. D., et al., in AIP Conf. Proc. 403, N.Y. (1997) p.327; SCHULTZ S. D., et al., in AIP Conf. Proc. 485, N.Y. (1999) p.317; SCHULTZ S. D., Ph.D. Thesis, Dpt. of Physics, M.I.T., (1999).
[2] SHKAROFSKY I. P. and SHOUCRI M., Nucl. Fusion, 37 539 (1997).
[3] PEYSSON Y. and SHOUCRI M., Comp. Phys. Comm. 109, 55 (1998).
[4] DECKER J. et al., in Proc. 12th Joint Workshop on EC Emission and EC Heating, Aix-en-Provence, France (2002).
[5] COPPI B. and SIGMAR D. J. , Phys. Fluids 16, 763 (1973).
[6] HINTON F. L. and HAZELTINE R. D., Rev. Mod. Phys. 48, 239 (1976).
[7] HIRSCHMAN S. P. , Phys. Fluids 31, 3150 (1988).
[8] SAUTER O. , et al., Phys. Plasmas 7, 2834 (1999).
[9] WESTERHOF E. and PEETERS A. G. , poster presented at the 35th Annual Meeting of the APS Division of Plasma Physics, St Louis, USA, (1993).
[10] JU M. et al., to be published in Phys. Plasma (2002).
[11] BONOLI P., et al., Nuclear Fusion 40, 1251 (2000).